Proceedings of the
Annual Stability Conference
Structural Stability Research Council
Pittsburgh, Pennsylvania, May 10-14, 2011

Towards a strain energy based strength prediction for locally slender structural steel columns

M.S. Seif[1], B.W. Schafer[2]

Abstract
The work presented herein is part of a continuing effort towards fully understanding the impact of local cross-section stability, including web-flange interaction, on structural steel strength. Locally unstable cross-sections at failure resist load through a complex nonlinear stress state in the cross-section. Here, the strain energy in the local buckling mode is explored as means to predict the underlying stress distribution at collapse. Through describing and analyzing a series of nonlinear shell finite element collapse analyses, previous efforts* provided comparisons of available design methods with expected capacities. Here the parametric studies previously created for the design comparisons are utilized to provide the stress distribution at failure of a wide variety of sections, and for further strength comparisons in the development of a strain energy based method. It is shown that for a plate the strain energy based method may be equated to traditional effective width (or direct strength) methods, but when extended to the cross-section the procedure provides unique strength predictions. Advantages and challenges with the strain energy based strength prediction method are explored. The method is shown to have significant promise, but further work is required.

1. Introduction
Through describing and analyzing a series of finite element (FE) analysis, previous efforts (see Seif and Schafer 2009 and 2010) provided comparisons of three design methods for locally slender steel short beams and stub columns; (i) AISC, and two methods from cold-formed steel specifications: (ii) AISI-Effective Width, and (iii) AISI-Direct Strength Method (DSM). In AISC, AISI, and DSM global column buckling is predicted using the same (single) expression. However, local-global interaction is handled by the Q-factor method in AISC, the unified method in AISI, and a variation of the unified method in DSM. In all cases the global strength is reduced due to local slenderness. The Q-factor approach reduces the strength and increases the long-column slenderness to arrive at its reduction. The unified method uses the effective area of the column at the long column buckling stress. DSM uses a similar approach.

[1] Graduate Research Assistant, Johns Hopkins University, <mina.seif@jhu.edu>
[2] Professor and Chair, Johns Hopkins University, <schafer@jhu.edu>

* *This research is a part of an AISC Faculty Fellowship: "Cross-section stability of structural steel", and is a continuation of presentations by Seif, M. and Schafer, B.W., presented in the 2009 and 2010 SSRC conferences.*

In the authors previous work, a nonlinear finite element (FE) analysis parameter study was carried out for the purpose of understanding and highlighting the parameters that lead to the divergence between the capacity predictions of the different design methods under axial and bending loads (Seif and Schafer 2009, 2010). Based on the authors' judgment, AISC W14 and W36 sections were selected for study as representing "common" sections for columns and beams in high-rise buildings. The W14x233 section is approximately the average dimensions for the W14 group and the W36x330 for the W36 group. All sections were modeled with globally pinned, warping fixed boundary conditions, and loaded via incremental displacement (columns) or rotation (beams).

To examine the impact of slenderness in the local buckling mode, and the impact of web-flange interaction in I-sections, four series of parametric studies were performed under axial and bending loading: **W14FI**: a W14x233 section with a modified Flange thickness, that varies Independently from all other dimensions, **W14FR**: a W14x233 section with variable Flange thickness, but the web thickness set so that the Ratio of the flange-to-web thickness remains the same as the original W14x233, **W36FR**: a W36x330 section with variable Web thickness, but the flange thickness set so that the Ratio of the flange-to-web thickness remains the same as the original W36x330, and **W36WI**: a W36x330 section with a variable Web thickness, that varies Independently from all other dimensions. Element thicknesses were varied between 0.05 in. (1.27 mm) and 3.0 in. (76.2 mm). While not strictly realistic, the values chosen were for the purposes of comparing and exercising the design methods up to and through their extreme limits.

ABAQUS was used to perform the analysis. Members were modeled using S4 shell elements. The material model follows classical metal plasticity: von Mises yield criteria, associated flow, and isotropic hardening. The uniaxial σ-ε diagram is provided in Fig. 1(a), and is similar to that employed by Barth et al. (2005). The curve is converted to a true σ-ε curve for the ABAQUS analysis. The classic and commonly used residual stress distribution of Galambos and Ketter (1959), as shown in Fig. 1(b), is employed. The residual stresses are defined in the finite element analysis as initial longitudinal stresses, and given as the average value across the element at its center (see e.g., Jung and White 2006).

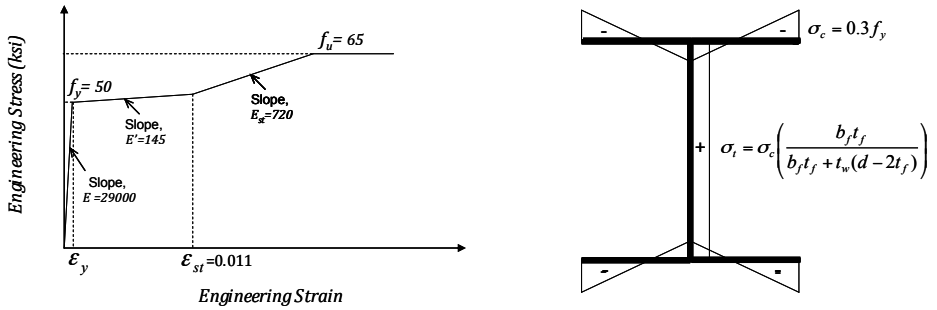

(a) uniaxial σ-ε relation (b) residual stress distribution

Figure 1: Idealized material model (a) σ-ε and (b) residual stresses

Initial geometric imperfections are added through linearly superposing a scaled local and a scaled global eigenmode solution from a finite strip analysis performed on each section, using CUFSM (Schafer and Ádány 2006). The local buckling mode is scaled so that the maximum

nodal displacement is equal to the greater of $b_f/150$ or $d/150$ (see, e.g. Kian and Lee 2002), while the global buckling mode is scaled so that the maximum nodal displacement is equal to $L/1000$.

Overall, the FE parameter study concluded that AISC's solutions are overly approximate for locally slender sections and deserve improvement, particularly for flanges (unstiffened elements). AISI's effective width, while the most complicated of the methods, appears to provide the most accurate solution, particularly for braced (stub) columns. The simplicity of DSM is obvious in the design expressions and resulting strength curves, but the elastic web-flange interaction assumed in the method is not always realized. DSM provides a consistently conservative, and conceptually simple prediction method that is worthy of further study. Such a study is initiated herein based on utilizing the strain energy in the local buckling mode shape.

2. Towards a Strain Energy Based Strength Prediction Method

Locally unstable cross-sections at failure involve a complex nonlinear stress-strain state in the cross-section. The Q-factor approach and existing DSM essentially ignore this stress state, while the unified (effective width) method simplifies the distributions to step functions based on stability of isolated elements in the cross-section. The previously conducted nonlinear FE analysis parameter study (Seif and Schafer 2009 and 2010) provides a database of failure mechanisms and stresses for W-sections at different element slenderness ratios. The main objective of this current work is to closely examine the stress distributions observed at failure, and consider a semi-empirical means for predicting these distributions utilizing the strain energy distribution of the cross-section local elastic buckling mode.

2.1. ABAQUS Finite Element Stress/Strain Distributions

Existing nonlinear FE analysis parameter studies, completed by the authors, provide the stress distribution at failure for a wide variety of W-sections. The first step completed is the conversion of the three-dimensional stress/strain distributions for the members into two-dimensional (cross-sectional) distributions. These two-dimensional stress distributions provide a direct means to estimate the "real" effective area. The main idea is illustrated in Fig. 1(a); however, one must take care because, as indicated in Fig 1(b), the two-dimensional S4 shell elements themselves have thickness (and integration points throughout the thickness). In this work the averaged longitudinal stress along the length and through the thickness was utilized for generating the two-dimensional stress distribution in the cross-section. Other options include considering critical cross-sections alone, or using only the shell element mid-surface values.

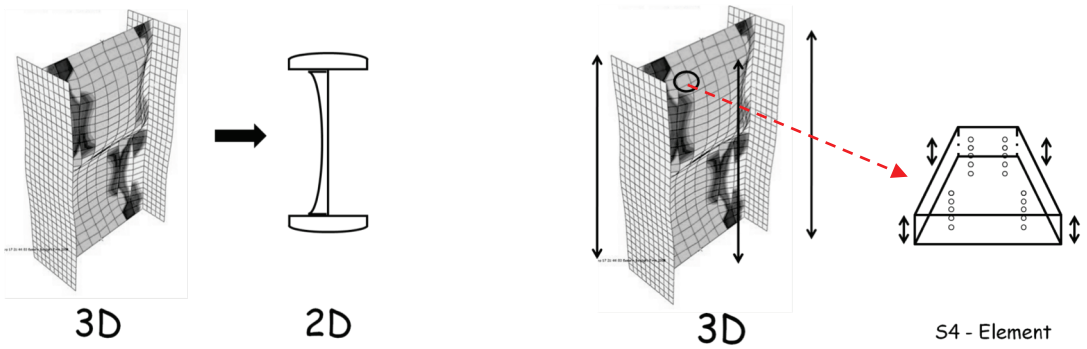

Figure 2: (a) Sketch showing the conversion of longitudinal 3D stresses into 2D (cross-sectional) stresses. (b) Averaging the stress/strain distributions along a member's length and through the element's thickness

As a check on the generated stresses the reported longitudinal stresses were integrated over the length and through the thickness and compared with the end reactions. Error, between 2% and 11% of the failure load was observed. The source of the error was traced to (i) difference between the deformed element longitudinal stress in local coordinates and global longitudinal stress, and (ii) a minor issue with the residual stress definition under small loads. The residual stresses were defined in the finite element analysis as initial longitudinal stresses, and given as the average value across the element at its center. For this distribution to be in equilibrium the average tension stresses in the web are computed in terms of the clear height (d-$2t_f$). However, this value was then applied to centerline models (height= d-t_f), thus leaving out a force equal to the tensile residual stress, σ_t, multiplied by the missing area: $2t_w$½t_f.

The averaged (over length and thickness) two-dimensional longitudinal stress at failure is shown for stub columns in the range of cross-sections studied in Fig. 3 – 6. Longitudinal stress is scaled so that the height of maximum stress value (~ 345 MPa or 50 ksi) is plotted at 10% of the cross-sectional height. The distribution of the stress at failure shows reductions in the center of the web and the flange tips in the thinnest W14 sections and in the W36 section when the web and flange are both reduced in thickness (W36FR). However, in all other cases the flange sees little to no reduction (carrying the full and uniform stress) while the web is significantly reduced.

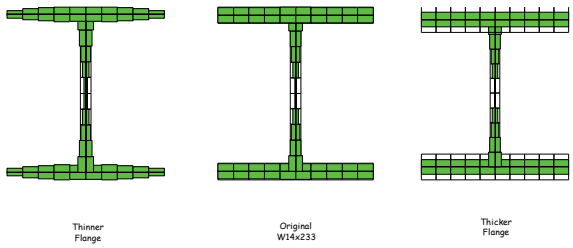

Figure 3: Samples of normalized longitudinal stress distributions in W14FI sections, max. stress ~f_y

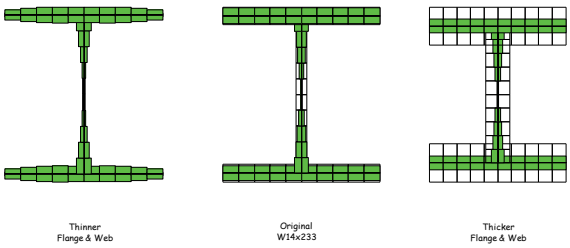

Figure 4: Samples of normalized longitudinal stress distributions in W14FRsections, max. stress ~f_y

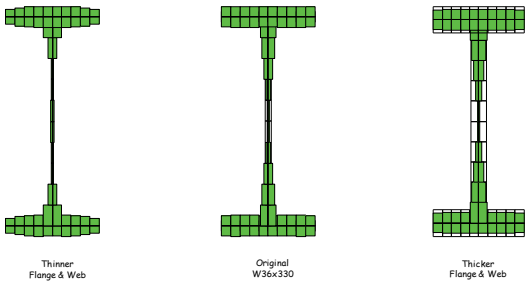

Figure 5: Samples of normalized longitudinal stress distributions in W36FR sections, max. stress ~f_y

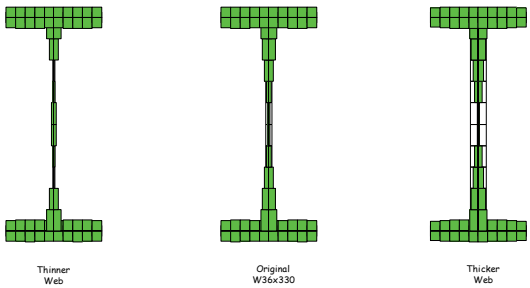

Figure 6: Samples of normalized longitudinal stress distributions in W36WI sections, max. stress ~f_y

2.2 Finite Strip Based Strain Energy Distributions

The cross-section strain energy distribution in the local buckling mode is examined as a potential tool for approximating effective area (stiffness). A typical finite strip analysis (from CUFSM) for a W36-section under axial loading is provided in Fig. 7. The inset of Fig. 7 shows the strain energy distribution associated with the local buckling mode. The visual similarity between the inverse of this energy distribution and the stress distribution at failure motivated much of the initial work herein.

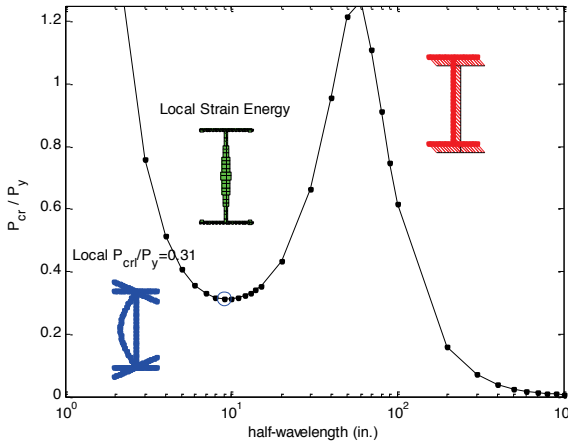

Figure 7: Typical CUFSM curve for a W36 slender section with mode, strain energy, and loading insets

For the four parametric studies conducted the strain energy distribution and the "inverse" of the bending strain energy distribution is provided on the following page (Fig. 8 – 15). Strain energy includes both bending strain energy and membrane strain energy (Schafer and Ádány 2006). Bending strain energy is associated with classic thin plate theory local buckling; and indeed is nearly 100% of the total strain energy for the thinner members studied (Fig. 8, 10, 12, 14). However, the thicker members include significant membrane strain energy. For comparison with the established stress distributions (Fig. 3-6) a re-normalized version of the bending strain energy is generated. Termed simply "1-SE" this re-normalized bending strain energy is the maximum bending strain energy minus the calculated bending strain energy (at every point). The resulting "1-SE" distributions are provided in Fig. 9, 11, 13, and 15.

In some cases the "1-SE" distribution is in good agreement with the longitudinal stress at failure; for example, the W36FR sections of Fig. 5 and 13. In other cases, the agreement is less convincing; for example, the W14FR sections of Fig. 4 and 11, where particularly for the thinnest sections the ratio of stress (or re-normalized stain energy) between the flange and web differs. In general the "1-SE" distributions do not differ markedly from the stress at failure, but the agreement is imprecise and the role of membrane strain energy is not directly reflected. Ultimately, it is concluded that the agreement is close enough to justify further consideration of "1-SE" distributions (bending only) as a proxy for the stress at failure, but further refinement is needed, as discussed in the next section.

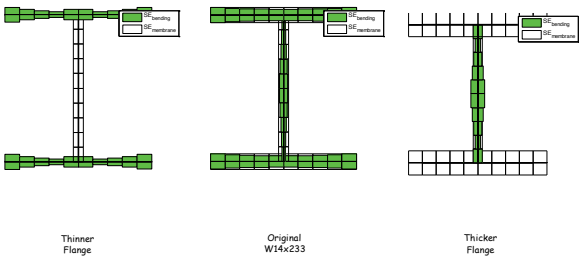

Figure 8: Strain energy distributions for the W14FI group under axial loading

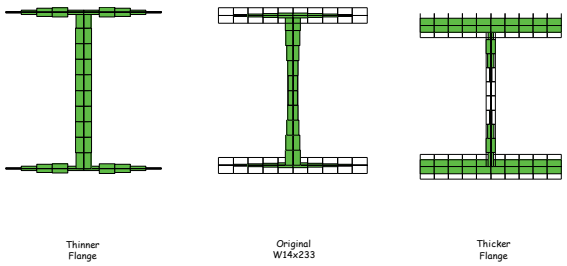

Figure 9: (1-SE) distributions for the W14FI group under axial loading as predicted by inverting the bending strain energy distribution

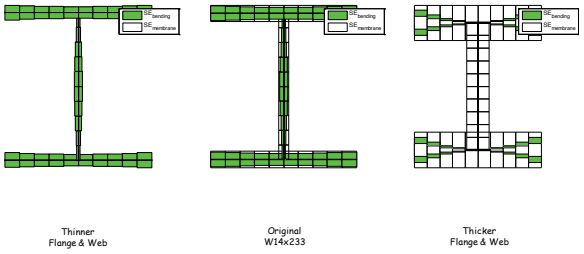

Figure 10: Strain energy distributions for the W14FR group under axial loading

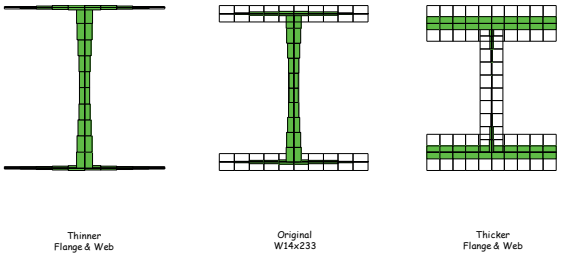

Figure 11: (1-SE) distributions for the W14FR group under axial loading as predicted by inverting the bending strain energy distribution

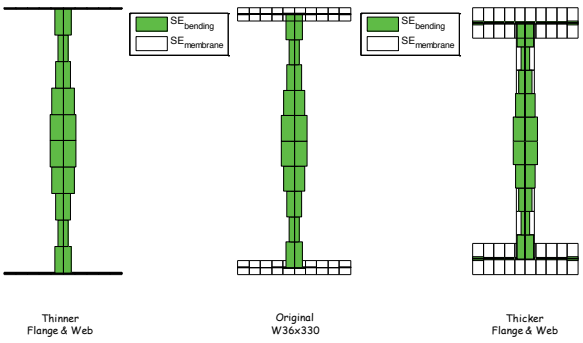

Figure 12: Strain energy distributions for the W36FR group under axial loading

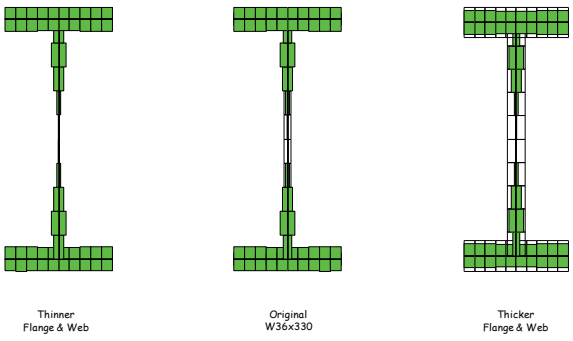

Figure 13: (1-SE) distributions for the W36FR group under axial loading as predicted by inverting the bending strain energy distribution

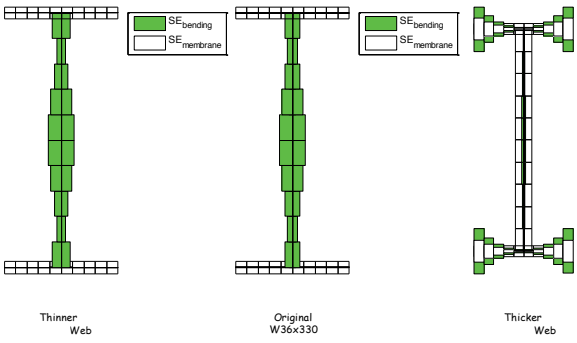

Figure 14: Strain energy distributions for the W36WI group under axial loading

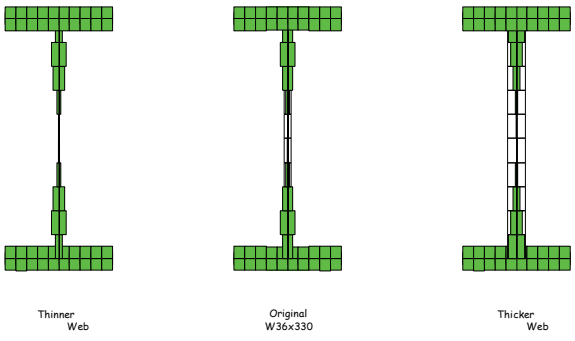

Figure 15: (1-SE) distributions for the W36WI group under axial loading as predicted by inverting the bending strain energy distribution

3. Towards Strain Energy Based Strength Prediction Method (SEM)

3.1 Strain Energy Based Prediction Methods for Plate Strength

The bending strain energy (*SE*) distribution indicates where large out-of-plane bending is expected in a plate. These regions are expected to have lower axial stiffness and yield on the faces of the plates first. Thus, in terms of effective thickness available to carry longitudinal stress, regions of high bending strain energy are regions of low effective stiffness/thickness. Therefore, it is postulated that an effective thickness distribution that is tied to the "1-*SE*" distribution may provide a more useful means of reducing the gross cross-section than traditional effective width methods.

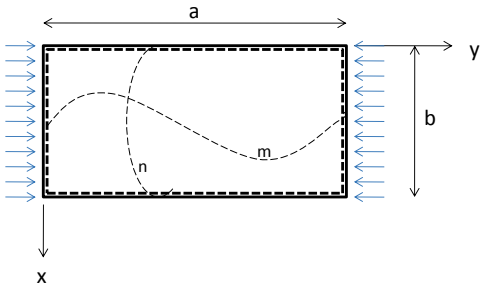

Figure 16: Simply supported plate loaded in the x-direction

Consider a simply supported plate with length, a, width, b, and thickness, t, loaded in the y-direction (Fig. 16). For simplicity, consider a square plate, a=b, (i.e. a locally buckled cell of a long plate).

For the traditional effective width method (subscript "*ewm*" herein), the effective width may be understood as a function, ω, that operates on the thickness, itself a function of plate slenderness:

$$P_{ewm} = \int_0^b \omega_{ewm} \cdot t \cdot f_y dx \tag{1}$$

where:

$$\omega_{ewm} = 1 \quad \text{for} \quad x \le \frac{1}{2} \cdot \rho \cdot b \quad \text{or} \quad x \ge b - \frac{1}{2} \cdot \rho \cdot b \tag{2a}$$

$$\omega_{ewm} = 0 \qquad \text{elsewhere.} \tag{2b}$$

The strain energy based method explored here replaces ω_{ewm} with a strain-energy based ω. Note, ρ of Eq. 2 is a function of local slenderness (i.e., Winter's equation, see Seif and Schafer 2009), and the final strength expression simplifies to:

$$P_{ewm} = \rho \cdot b \cdot t \cdot f_y \tag{3}$$

Returning to the plate of Fig. 16, and assuming the displacement function is:

$$w = A \cdot \sin\left(\frac{n\pi x}{b}\right) \cdot \sin\left(\frac{m\pi y}{a}\right) \tag{4}$$

one can find the bending strain energy (SE) distribution along the side for a square plate, a=b, in the first mode m=n=1 as:

$$SE = \frac{A^2 \cdot D \cdot \pi^4}{4 \cdot b^5} \cdot (1+\nu) \cdot \sin\left(\frac{\pi x}{b}\right)^2 \tag{5}$$

This may be normalized so that the maximum *SE* across the width is 1.0:

$$\frac{A^2 \cdot D \cdot \pi^4}{4 \cdot b^5} \cdot (1+\nu) = 1.0 \tag{6}$$

$$A^2 = \frac{4 \cdot b^5}{D \cdot \pi^4 \cdot (1+\nu)} \tag{7}$$

Finally, substituting in for *A,* one finds the normalized strain energy distribution (max 1.0):

$$SE_n = \sin\left(\frac{\pi x}{b}\right)^2 \tag{8}$$

The basic effective width distribution (ω_{ewm}) is [0,1], i.e., heavy-side functions that are switched on/off as a function of effectiveness (ρ) or equivalently slenderness, λ, (i.e. f_{cr} and f_y). The SE distribution is continuous and here 1-SE_n is employed.

$$\omega_1 = 1 - SE_n \qquad \text{or} \qquad \omega_1 = 1 - \sin\left(\frac{\pi x}{b}\right)^2 \tag{9}$$

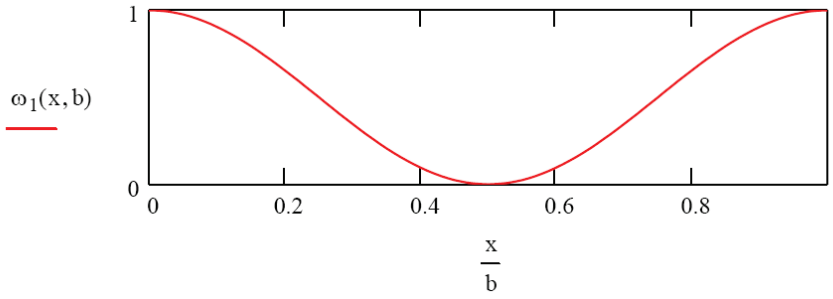

Figure 17: Strain energy distribution along a side of a square plate

The distribution of Eq. 9, i.e. Fig. 17, leads to only one predicted effective thickness (or strength). The expression ultimately needs a parameter that is a function of slenderness, similar to the variable width in the effective width method, consider an expanded form of ω:

$$\omega(x, b, \alpha) = \left(1 - \sin\left(\frac{\pi x}{b}\right)^2\right)^{\alpha} \tag{10}$$

As α is varied a range of strength (effective thickness) predictions result, see Fig. 18. Thus:

$$P_1 = \int_0^b \left(1 - \sin\left(\frac{\pi x}{b}\right)^2\right)^{\alpha} \cdot t \cdot f_y dx \tag{11}$$

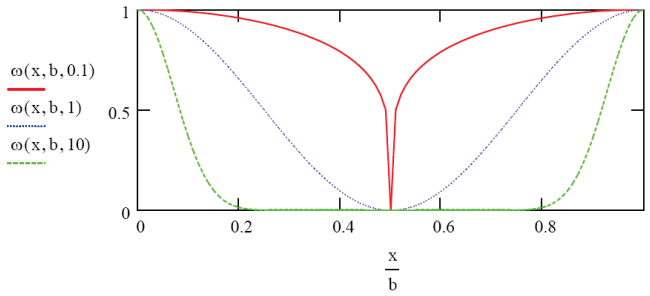

Figure 18: Range of strain energy distributions along a side of a square plate as function of α

As a means to initially calibrate the new strain energy based strength prediction method (SEM), SEM strength is set equal to the effective width prediction. Thus, for an isolated plate, the two methods will yield similar capacities, but for members, this approach is quite different. Now equating Eq. 3 and Eq. 11, one can solve for ρ in terms of α as follows:

$$\rho(\alpha) = \frac{1}{b}\int_0^b \left(1 - \sin\left(\frac{\pi x}{b}\right)^2\right)^{\alpha} dx \tag{12}$$

A closed-form solution for α in terms of ρ is not readily possible, so an approximation of the following functional form is explored:

$$\rho_a(\alpha) = \frac{c}{\alpha^a + c} \tag{13}$$

which may be solved for α as:

$$\alpha = \left(\frac{c}{\rho} - c\right)^{a^{-1}} \tag{14}$$

Eq. 13/14 is an approximation between fit and accuracy. Fig. 19 provides the accuracy of Eq. 13 for a chosen exponent a=0.8 and coefficient c=1.1, when compared to Eq. 12. Also, Fig. 20 shows the accuracy of normalized P_n for the same values of a and c.

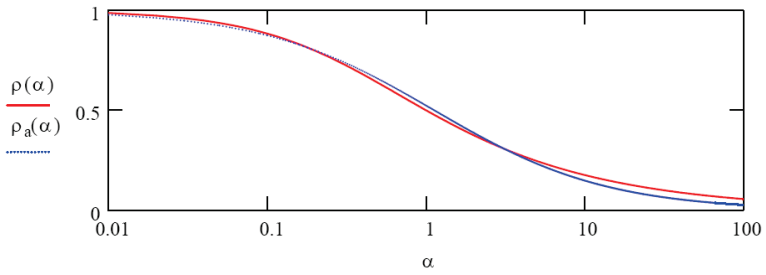

Figure 19: Numerical approximation for ρ versus the real value

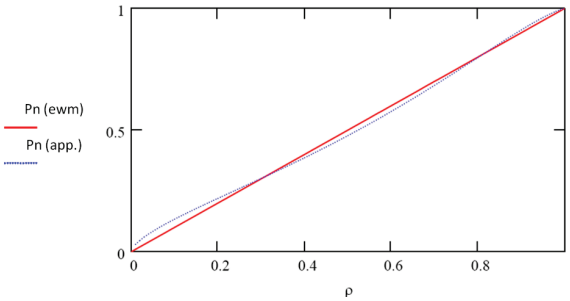

Figure 20: Normalized strength prediction accuracy

3.2 Extending the Strain Energy Based Prediction Method to Columns

The Strain Energy based prediction method (SEM) explored herein for a column without distortional buckling, is a new hybrid of the Direct Strength Method (DSM) and Effective Width Method (EWM). The strength reductions due to local buckling are based on local cross-section slenderness and analysis (i.e., not just the elements, so this is consistent with DSM), but the application of the reductions reduce properties around the section (and thus shares similarities with the effective width method). SEM is explored in the following form. First one finds the stress in global flexural, torsional, or torsional-flexural buckling, F_{ne}:

$$\text{for } \lambda_c \le 1.5 \quad F_{ne} = \left(0.658^{\lambda_c^2}\right) F_y, \quad \text{and} \tag{15.a}$$

$$\text{for } \lambda_c > 1.5 \quad F_{ne} = \left(\frac{0.877}{\lambda_c^2}\right) F_y = 0.877 F_{cre} \tag{15.b}$$

where $\lambda_c = \sqrt{F_y / F_{cre}}$, F_y = yield stress, and F_{cre} = minimum of the critical elastic column buckling stress in flexural, torsional, or torsional-flexural buckling. Note, for a fully braced column $F_{ne} = F_y$. Next the reduction factor due to local buckling is determined as ρ_ℓ, via:

$$\text{for } \lambda_\ell \le 0.776 \qquad \rho_{\ell 1} = 1.0 \text{ , and} \tag{16.a}$$

$$\text{for } \lambda_\ell > 0.776 \qquad \rho_{\ell 1} = \left(1 - 0.15\left(\frac{F_{cr\ell}}{F_{ne}}\right)^{0.4}\right)\left(\frac{F_{cr\ell}}{F_{ne}}\right)^{0.4} \tag{16.b}$$

alternatively, instead of the DSM reduction factor, Winter's (EWM's) factor may be used:

$$\text{for } \lambda_\ell \le 0.673 \qquad \rho_{\ell 2} = 1.0 \text{ , and} \tag{17.a}$$

$$\text{for } \lambda_\ell > 0.673 \qquad \rho_{\ell 2} = \left(1 - 0.22\left(\frac{F_{cr\ell}}{F_{ne}}\right)^{0.5}\right)\left(\frac{F_{cr\ell}}{F_{ne}}\right)^{0.5} \tag{17.b}$$

where $\lambda_\ell = \sqrt{F_{ne} / F_{cr\ell}}$, and $F_{cr\ell}$ = critical elastic local column buckling load. Now, to determine how to apply the reduction on the cross-section the bending strain energy is employed. Specifically, if *SE* is equal to the bending strain energy distribution around the cross-section for the local mode shape at $L_{cr\ell}$: (a) normalize *SE* so that the max(*SE*) = 1.0, (b) take 1-*SE* as the base distribution in the section, ω, and (c) use the shape parameter, α, tied to the local reduction factor (ρ_ℓ) to determine the effective thickness and area. Specifically:

$$A_{eff} = \int_0^S \omega^\alpha t ds \cong \sum_i b_i \omega_i^\alpha t, \tag{18}$$

$$\omega = (1 - SE) \tag{19}$$

where s is the perimeter length of a cross-section – practically this will always be broken into i segments and the mesh used in the FSM analysis to determine the elastic buckling stress would conveniently define the i segments (i.e. the width of the strips). Based on preliminary work in the previous section, for α, two expressions are explored:

$$\alpha_1 = \frac{c}{\rho_\ell} - 1 \quad \text{, and} \tag{20}$$

$$\alpha_2 = \left(\frac{1.1}{\rho_\ell} - 1.1 \right)^{\frac{1}{0.8}} \tag{21}$$

Finally, the strength prediction based on this approach is

$$P_{n\ell SE} = A_{eff} F_{ne} \tag{22}$$

Where, depending on the choice of ρ_ℓ and α, four options exist for exploration:

$$\begin{aligned} P_{n\ell SE-11} &= A_{eff}(\alpha_1, \rho_{\ell 1}) F_{ne} \\ P_{n\ell SE-12} &= A_{eff}(\alpha_1, \rho_{\ell 2}) F_{ne} \\ P_{n\ell SE-21} &= A_{eff}(\alpha_2, \rho_{\ell 1}) F_{ne} \\ P_{n\ell SE-22} &= A_{eff}(\alpha_2, \rho_{\ell 2}) F_{ne} \end{aligned} \tag{23}$$

Note, α_1 is strongly preferred for its simplicity. In the following plot, Fig. 21, for a sample locally slender W-section, a more detailed look at the buckling mode, the strain energy, the distribution $\omega = 1 - SE$, and at $F_{ne} = F_y$, the effective thickness is provided. While Fig. 21 provides ω and t_{eff}, a key feature of the developed method is the ability to shape ω when creating t_{eff}, specifically ω^a is the effective thickness and α is a function of the traditional slenderness parameter ρ. Fig. 22 shows t_{eff} for ρ varying from 0.25 to 1.0. Fig. 22 illustrates that the method has the potential to go from a strongly reduced cross-section up to a fully effective section – all while utilizing 1-SE as the basis for the distribution.

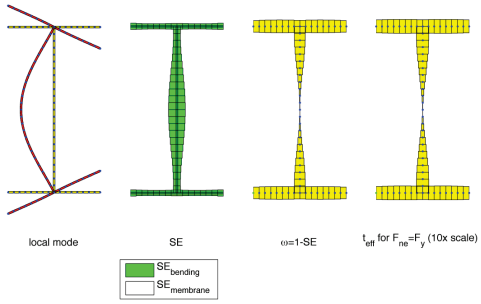

Figure 21: Buckling mode, strain energy, ω=1-SE, and effective thickness for a locally slender W36 section

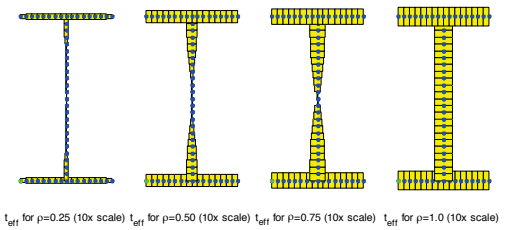

Figure 22: Effective section area for a locally slender W36 section for ρ varying from 0.25, 0.5, 0.75 and 1.0

Fig. 23 provides a column curve comparison between the original DSM predictions, and the predictions calculated by the four proposed SEM variations for (a) the original W14x233 section under axial loading and (b) the original W36x330. In both cases the SEM variations provide essentially the same prediction as DSM. To explore regimes where the differences are accentuated the thinnest sections of the FE parametric studies are examined next.

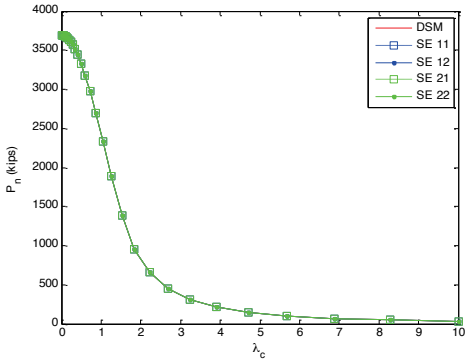

(a) W14x233

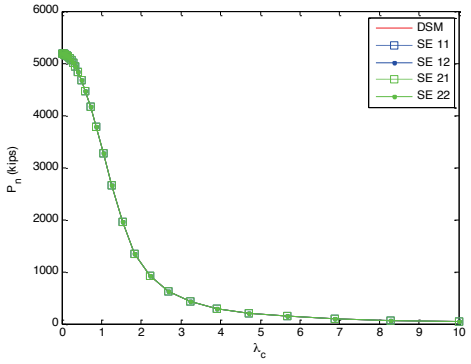

(b)W36x330

Figure 23: Column curve by DSM and SEM method for conventional W14 and W36

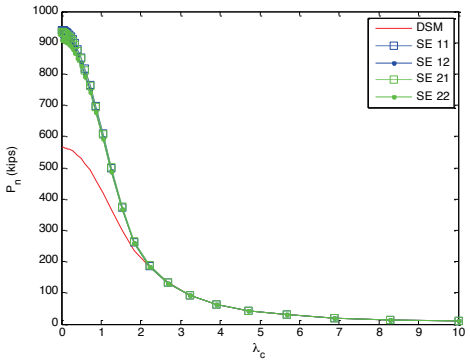

(a) thin (extreme local slenderness) W14FI section

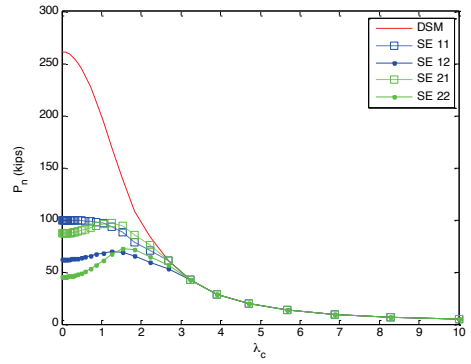

(b) thin (extreme local slenderness) W14FR section

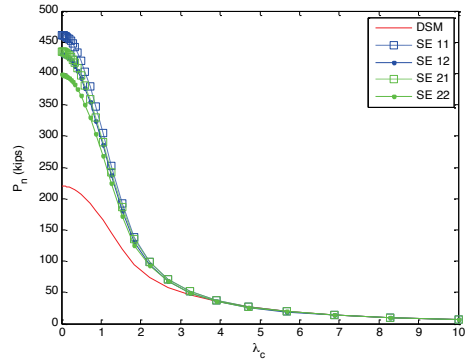

(c) thin (extreme local slenderness) W36FR section

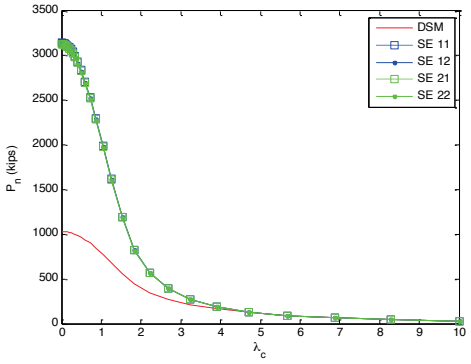

(d) thin (extreme local slenderness) W36WI section

Figure 24: Column curves by DSM and SEM for thin (locally slender) sections in each parameter study

Strength results for column curves of the sections with extremely high local slenderness (i.e., very thin, variable thickness = 0.15in.) for the four study groups: W14FI, W14FR, W36FR, and W36WI are provided in Fig. 24. For the W14FI, W36FR, and W36WI the SEM strength predictions are significantly greater than DSM at short lengths, and closer to ultimate capacities

predicted by ABAQUS nonlinear shell element collapse analysis (Seif and Schafer 2009, 2010). However, for the W14FR section SEM predicts lower capacities than DSM or ABAQUS nonlinear shell element collapse analysis; indicating potential fundamental difficulties with application of the 1-*SE* distribution in predicting the stress at failure in every case.

Complete comparisons for the SEM method (P_{11}) with ABAQUS nonlinear shell element collapse analysis and existing design methods, for stub columns, plotted as a function of local slenderness, across all four parameter study groups is provided in Fig. 25. It is observed that (i) SEM generally performs well, except for the W14FR study group, (ii) SEM, as implemented, has a pronounced drop in strength in the transition to partially effective sections, a drop not reflected in the collapse analysis.

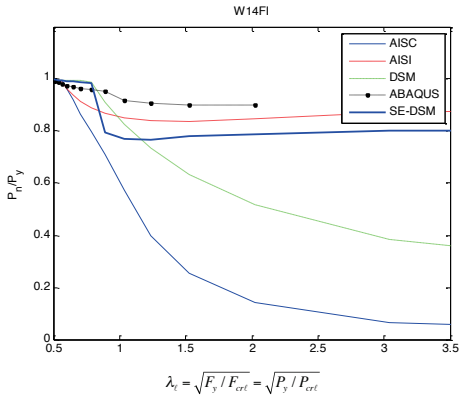

(a) W14FI stub columns (varying local slenderness)

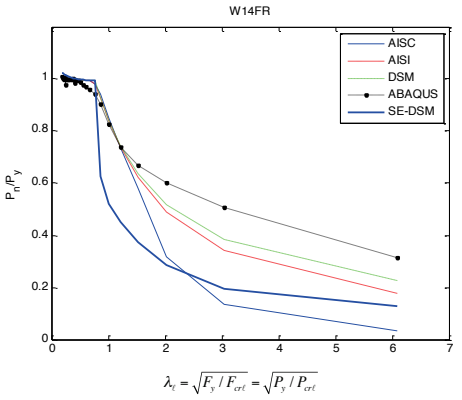

(b) W14FR stub columns (varying local slenderness)

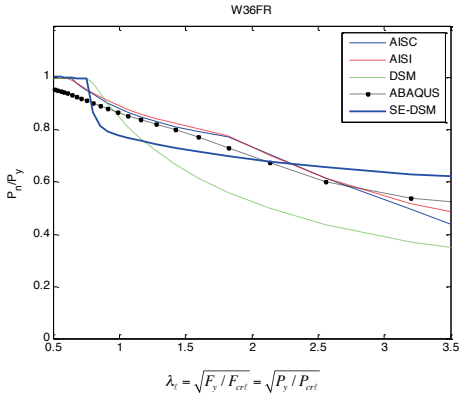

(c) W36FR stub columns (varying local slenderness)

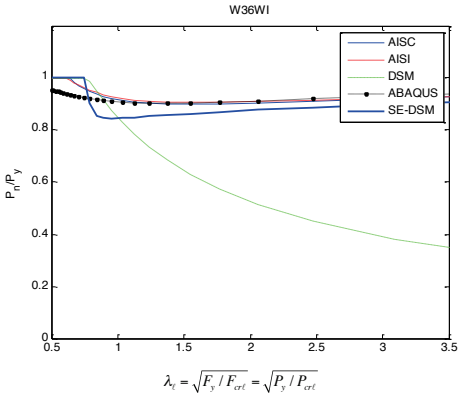

(d) W36WI stub columns (varying local slenderness)

Figure 25: Results of stub column parametric study for 3 design methods versus SEM

The strain energy based prediction method (SEM) proposed herein shows promise as a general method for predicting the strength of locally slender sections where elements of the cross-section have strong differences in slenderness. Further, effective properties (I, C_w, etc.) based on the SE-based effective thickness reductions would be simple to calculate and have significant potential for their use in high efficiency frame element analysis with reduced (effective) properties. A variant of the original unified effective width method (more like the Q-factor approach) that uses the effective moment of inertia in the global column expression (instead of effective area) is worth pursing with the SEM approach. SEM still requires greater refinement as (i) in some cases it may result in overly conservative solutions, (ii) the implementation provided herein may reduce the strength too sharply in the transition to partially effective sections, and (iii) membrane

strain energy is not yet incorporated in the method. Nonetheless, the overall approach provides a potentially fruitful new direction for semi-empirical design methods.

4. Conclusions

The stress distribution of a locally slender structural steel cross-section at collapse is a complex nonlinear function. The stress at failure for a larger parametric study of modified W14 and W36 structural steel column cross-sections was predicted using nonlinear shell finite element collapse analysis in ABAQUS. Correlations between the stress distribution at failure, reduced (averaged) to its cross-section distribution, and the bending strain energy in the local buckling mode are observed. Specifically, regions of high bending strain energy in the local buckling mode correspond to regions of low stress at collapse. Using this correlation it is postulated that the strain energy distribution (appropriately normalized) may be used to determine effective cross-section thickness in local buckling modes. For an isolated plate this new strain energy based prediction method (SEM) is derived such that it provides predictions equivalent to the Effective Width Method, or alternatively, the Direct Strength Method (DSM). Extension of the SEM approach to cross-section strength prediction demonstrates the promise of the method – results are much improved over DSM for three of the four parametric study groups. Also, areas in need of improvement are highlighted – one study group (of W14 sections where the flange/web ratio is held constant but the thickness varied) is grossly conservative. The SEM approach provides a potential means to provide cross-section specific strength predictions, tied to full cross-section elastic buckling analysis, but without the time or expense of nonlinear collapse analysis. Though still under development, preliminary results provided here indicate further work on strain energy based methods is warranted.

Acknowledgments

The authors of this paper gratefully acknowledge the support of the AISC, and the AISC Faculty Fellowship program in this research. Any views or opinions expressed in this paper are those of the authors.

References

AISC (2005). “Specification for Structural Steel Buildings”, American Institute of Steel Construction, Chicago, IL. ANSI/ASIC 360-05.

AISI (2007). “North American Specification for the Design of Cold-Formed Steel Structures”, Am. Iron and Steel Inst., Washington, D.C., AISI-S100.

Barth, K.E. et al (2005). “Evaluation of web compactness limits for singly and doubly symmetric steel I-girders”, *J. of Constructional Steel Research* 61 (2005) 1411–1434.

Galambos, T.V., Ketter, R.L. (1959). “Columns under combined bending and thrust”, *Journal Engineering Mechanics Division*, ASCE 1959; 85:1–30.

Jung, S., White, D.W. (2006). “Shear strength of horizontally curved steel I-girders—finite element analysis studies”, *J. of Const. Steel Research* 62 (2006) 329–342.

Kim, S., Lee, D. (2002). “Second-order distributed plasticity analysis of space steel frames”, *Engineering Structures* 24 (2002) 735–744.

Schafer, B.W., Ádány, S. (2006). “Buckling analysis of cold-formed steel members using CUFSM: conventional and constrained finite strip methods.” Proceedings *of the Eighteenth International Specialty Conf. on Cold-Formed Steel Structures*, Orlando, FL. 39-54.

Seif, M., Schafer, B.W. (2009). “Finite element comparison of design methods for locally slender steel beams and columns”, *SSRC Annual Stability Conference Proceedings*, Phoenix, AZ, April 2009, p. 69-90.

Seif, M., Schafer, B.W. (2010). “Design methods for local-global interaction of locally slender steel members”, *SSRC Annual Stability Conference Proceedings*, Orlando, FL, May 2010, p.553-572.